PAPER

Check for updates

Residence time distribution effects on continuous-flow reaction in a polymer gel-based porous monolith: investigation of an asymmetric reaction with supported Hayashi–Jørgensen catalysts†

Harutaka Shigeeda, Hikaru Matsumoto, (iD) Masanori Nagao (iD) and Yoshiko Miura (iD)*

Immobilized catalysts are easy to reuse and applicable to continuous-flow reactions, but their catalytic activity decreases due to poor diffusivity of reactants. To mitigate the molecular diffusion resistance, it is important to design support materials that boost the diffusion of reactants toward the catalyst. Gels are polymers consisting of cross-linked networks that swell in aqueous and/or organic solvents. The gels are insoluble, like solids, but create a unique reaction environment within the network, where the molecular diffusivity is quite fast, as in a homogeneous system. In this respect, monolithic porous gels (**MPG**s) composed of organic polymer have been developed for continuous-flow reactors to mitigate the diffusion resistance of the reactants. However, the effects of the gel properties (*e.g.* cross-linking structure) on the molecular diffusivity through the **MPG** under continuous-flow conditions have not been quantitatively evaluated so far. Here, we prepared **MPG**s supporting Hayashi–Jørgensen catalysts and assessed the diffusivity within the gel on the basis of the residence time distribution, as well as on the catalytic performance in Michael addition reactions. The **MPG** with low cross-linking density exhibited a high swelling porosity ($\varepsilon_{\text{swollen}}$), which corresponded to fast molecular diffusion of the reactants. The **MPG** with the lowest cross-linking density demonstrated the highest diffusivity and superior turnover frequency ($\varepsilon_{\text{swollen}} = 100\%$, TOF = 2.4 h^{-1}) in the continuous-flow reactions.

Introduction

In recent years, continuous-flow synthesis of fine chemicals has garnered significant interest.[1–3] In continuous-flow systems, efficient heat and mass transfer, precise control of production amounts, automation, and safe operation can be achieved, offering many advantages over batch systems.[4,5] Asymmetric reactions are important chemical transformations for fine chemicals, such as pharmaceuticals, agrochemicals, and fragrances.[6,7] For efficient asymmetric reactions under continuous-flow conditions, immobilized catalysts supporting chiral molecules have attracted much interest. Since the catalysts are retained in the continuous-flow reactor, catalytic reaction and separation of products from the catalyst are achieved simultaneously, resulting in high process efficiency.

For continuous-flow reactions using immobilized catalysts, porous materials have emerged as promising supports. Due to the large surface area and high porosity of these porous materials, fast mass transport and efficient catalytic reactions have been realized.[8,9] Among these, porous monoliths provide a single support with a flow-through pore network.[10,11] The monoliths have flow-through macropores that allow fast permeation of fluid. Owing to the narrow pore-size distribution, mass transport of solutes through the macropores is relatively uniform and close to an ideal plug flow. These characteristics of monolith reactors are advantageous compared with packed-bed reactors.[12] Moreover, it has been reported that the formulation of micro/mesopores on the monolith surface provides a hierarchical porous structure, which increases the number of active sites and hence the catalytic efficiency.[13–15] Since the micro/mesopores are primarily accessible by diffusion, the mass transport of reactants in these pores is severely limited by diffusion resistance. As a result, some catalysts located on these pores are virtually inaccessible under continuous-flow conditions. In this case,

Department of Chemical Engineering, Kyushu University, 744 Motooka, Nishi-ku, Fukuoka 819-0395, Japan. E-mail: miuray@chem-eng.kyushu-u.ac.jp

† Electronic supplementary information (ESI) available. See DOI: https://doi.org/10.1039/d4re00597j

introduction of micro/mesoporosity into the monoliths will not directly improve the reactor performance as expected, due to the low catalytic efficiency in the unavailable pores. To enhance catalytic efficiency and reactor performance, porous monolith catalysts with fast molecular diffusion into the micro/mesopores are needed.

Gels are polymer materials consisting of cross-linked networks that swell in good solvents. The gels are insoluble in the solvents and exhibit similarly to solid materials. Furthermore, the swollen network of the gel provides microporosity toward small solutes, which facilitates molecular diffusion in the matrix.[16,17] It has been reported that solute diffusion through the gel can be considered to be as high as that in a solution.[18] These unique features depend on the physical properties of the gel, which vary with the cross-linking structure. To date, polymer gel catalysts have been developed as immobilized catalysts for asymmetric reactions, which show easy recoverability and excellent catalytic efficiency.[19–21] However, applications of gel catalysts to continuous-flow asymmetric reactions are scarce.[22]

In this respect, our research group has developed monolithic porous gels (**MPG**s), which are applicable to continuous-flow catalytic reactions. The **MPG**s are porous monoliths consisting of polymer gels that swell in the reaction media (Fig. 1). The **MPG**s have not only macropores, but also micropores, derived from the swollen gel network. This hierarchical porous structure of the **MPG** gives two different pathways for reactants. In the macropores, the reactants flow by convection of the reaction media. At the same time, the reactants rapidly transfer into the gel matrix by diffusion during the flow. As catalysts are immobilized in the gel network, the reactants can easily contact with the catalysts to form the desired products. Finally, the desired products diffuse out from the gel network and flow out of the reactor. Using the **MPG**s, excellent catalytic efficiencies have been realized in Suzuki–Miyaura cross-couplings[23,24] and asymmetric aldol additions[25] featuring fast molecular diffusion in the gel network. It is expected that the physical properties of the gel network in the **MPG**s contribute greatly to the accessibility toward the catalysts, and should vary with the cross-linking structure of the gel. Investigation of flow behavior through **MPG**s with different cross-linking structures would give insight into the mass transport in the continuous-flow reaction. However, quantitative studies on the effect of the cross-linking structure of **MPG**s on their catalytic performance have not been investigated so far.

In this study, a series of the **MPG** reactors with different cross-linked structures was prepared, and the correlation between mass transport phenomena and catalytic performance was investigated (Fig. 1). As a model catalyst, the Hayashi–Jørgensen catalyst (HJ-cat) was chosen because of its broad applicability and high durability in asymmetric synthesis of important fine chemicals, such as γ-amino acid derivatives.[26–28] Through copolymerization of the styryl monomer carrying HJ-cat (HJ-cat monomer), styrene, and divinylbenzene (DVB), an **MPG** supporting the HJ-cat was prepared. Owing to the flexibility of the polystyrene chains, this **MPG** swelled in organic solvents, such as toluene. In addition, varying the feed ratio of the DVB as a cross-linker provided **MPG**s with different degrees of cross-linking, which would show different swelling abilities in the organic solvent. For the flow behavior in the **MPG**s, the residence time distribution (RTD) was evaluated by pulse tracer experiments, which were correlated with the catalytic performance in the asymmetric Michael addition of propionaldehyde to trans-β-nitrostyrene under continuous-flow conditions.

Experimental

General

The samples for field emission scanning electron microscopy (FE-SEM) analysis were coated with platinum (approx. 4 nm thickness) using a JEOL JFC-1600 auto fine coater (JEOL Ltd., Tokyo, Japan). FE-SEM analysis was performed on a Hitachi SU8000 microscope (Hitachi High-Technologies Corporation, Tokyo, Japan). Mercury intrusion porosimetry (MIP) analysis was performed on a Micromeritics AutoPoreIV9520 (Micromeritics Instrument Co., Norcross, GA, USA). Elemental analysis (EA) was performed on a Yanako MT-6 CHN recorder (Yanaco Technical Science Co., Ltd., Tokyo, Japan). Solution nuclear magnetic resonance (NMR) spectra were recorded on a JEOL ECZ400S spectroscopy, operating at 400 MHz for ^{1}H NMR. Chemical shift values for the ^{1}H NMR spectra were referenced to Me$_4$Si. High-performance liquid chromatography (HPLC) analyses were performed on a JASCO LC-2000Plus system equipped with a JASCO DG-980-50 degasser, a JASCO PU-980 pump, a Kanto Chemical Mightysil RP-18 GP 250-4.6 column (Kanto Chemical Co., Tokyo, Japan), a JASCO UV-2077Plus UV detector, and a JASCO CO-2065Plus column oven (JASCO Co., Tokyo, Japan). Acetonitrile/water (60 : 40 v/v) containing trifluoroacetic acid
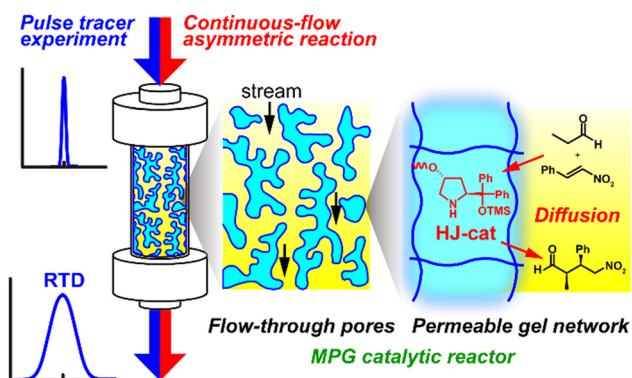

Fig. 1 Schematic of continuous-flow reactors using **MPG**s with different degrees of cross-linking. Mass transport of the reactants was estimated based on the RTD through the **MPG** reactors.

This journal is © The Royal Society of Chemistry 2025

React. Chem. Eng., 2025, **10**, 1038–1047 | **1039**

(0.1 vol%) was employed as a mobile phase in the HPLC measurements (1.0 mL min^{-1}). HPLC analyses for enantiomeric excess were performed on a JASCO LC-2000Plus system equipped with a JASCO DG-980-50 degasser, a JASCO PU-986 pump, a CHIRALPAK OD-H 250-4.6 column (Daicel Co., Osaka, Japan), a JASCO MD-4010 photo diode array detector, and a JASCO CO-2060Plus column oven (JASCO Co., Tokyo, Japan). 2-Propanol/hexane (6.2 : 93.8 v/v) was employed as a mobile phase in the HPLC measurements (0.75 mL min^{-1}).

In the continuous-flow setup, an SGE glass gas-tight syringe (SGE Analytical Science Pty. Ltd., Melbourne, Australia), which was mounted on a YMC YSP-101 syringe pump (YMC Co. Ltd., Kyoto, Japan), and a Krone KDM-30 pressure gauge (Krone Co., Tokyo, Japan) were connected to the column with PTFE or PFA tubing (0.75 mm inner diameter) in a thermo-controlled incubator. For RTD studies, a FLOM VI-11 injection valve (FLOM Co., Tokyo, Japan) with a 10 μL loop, an Ocean Optics USB2000+ ultraviolet-visible (UV-vis) spectrometer (Ocean Optics Inc., Dunedin, FL, USA), an Ocean Optics tungsten halogen light source (Ocean Optics Inc.), and an FIA-Z-SMA-TEF Z-type flow cell (Ocean Optics Inc.) were included in the continuous-flow setup.

Materials were obtained from commercial suppliers unless otherwise noted. Styrene (>99.0% GC purity, stabilized with 4-*tert*-butylcatechol, Tokyo Chemical Industry Co., Ltd., Tokyo, Japan) and divinylbenzene (DVB) (3- and 4- mixture, contains ethylvinylbenzene and ethylbenzene, >50.0% GC purity, stabilized with 4-*tert*-butylcatechol, Tokyo Chemical Industry Co., Ltd.) were purified using a basic alumina column. 2,2′-Azo-bis(isobutyronitrile) (AIBN) (98.0% absorptiometry purity, FUJIFILM Wako Pure Chemical Co., Osaka, Japan) was purified by recrystallization from MeOH. The HJ-cat monomer was synthesized according to previous reports (Fig. S1, see ESI† for details).[29]

Preparation and characterization of MPGs

HJ-cat monomer (10 wt%), DVB (X = 20, 40, or 60 wt%), and styrene (90–X wt%) were used as the catalyst moiety, cross-linker, and gel matrix monomers, respectively (Scheme 1a and b). The total weight of these monomers was 300 mg. The monomers were admixed with a mixture solvent of toluene/1-decanol (30 : 70 w/w, 700 mg) and completely dissolved by shaking. AIBN (3 mg, 1 wt% with respect to the monomers) was added to the mixture and completely dissolved. The resulting monomer solution was degassed by N$_2$ bubbling for 30 min and poured into a home-made column (stainless steel, 4.4 mm inner diameter (d) × 5.0 cm length (L)). After sealing with stainless steel plugs at both column ends, the column was heated in an incubator at 70 °C for 72 h. After the polymerization, the **MPG** column was washed by permeation of tetrahydrofuran (THF) for more than 1 h
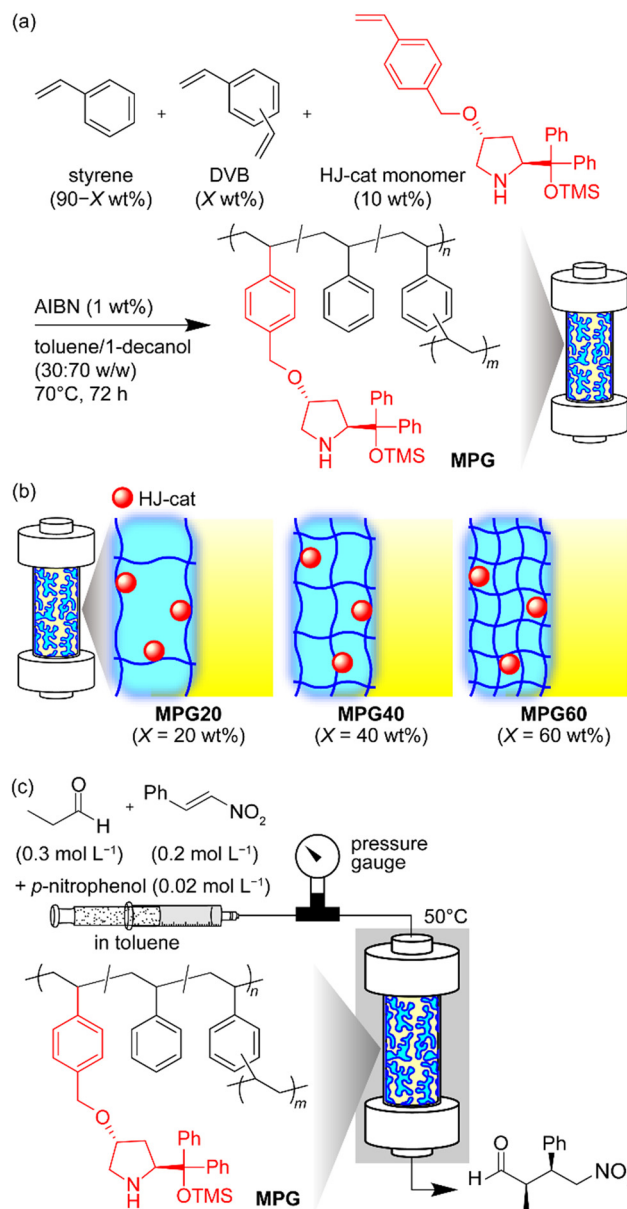
Scheme 1 (a) Synthesis of **MPG** supporting HJ-cat. (b) Preparation of **MPG**s with different cross-linking degree. (c) Continuous-flow setup for asymmetric Michael addition of propionaldehyde to *trans*-β-nitrostyrene.

(2.972 mL h^{-1}). For characterization of the **MPG**, the **MPG** was dried under vacuum and extruded from the column to give white solids.

Permeability test for continuous-flow reactors

After polymerization and washing with THF, the **MPG** column was connected to the syringe pump and pressure gauge. Superficial velocity (u) was defined as follows:

$$u = \frac{Q}{\pi d^2/4} \quad (1)$$

1040 | *React. Chem. Eng.*, 2025, **10**, 1038–1047

This journal is © The Royal Society of Chemistry 2025

where Q is the flow rate of the feed. As a mobile phase, toluene was permeated through the **MPG** at various u, and the pressure loss (ΔP) was monitored. At steady state, the Darcy's permeability (k_D) of the **MPG** was estimated as follows:

$$k_D = \frac{\mu L u}{\Delta P} \tag{2}$$

where μ is the viscosity of the feed solution.

Pulse tracer experiment for continuous-flow reactors

RTD in the continuous-flow system was evaluated using a pulse tracer. The **MPG** column was provided with fittings and attached to a syringe pump, injection valve of tracer, UV-vis spectrometer, deuterium halogen light source, and Z-type flow cell.[30] As a mobile phase, toluene was continuously permeated through the **MPG** column (Q = 0.743 mL h^{-1}). Methyl red (in EtOH, 1 g L^{-1}) as a pulse tracer (10 μL) was injected into the stream from the injection valve. At the outlet of the column, UV-vis absorbance at 427-nm wavelength at each time (t) was measured to monitor the concentration of the tracer in the eluent ($C(t)$). RTD function ($E(t)$) and residence time (τ) were calculated as follows:

$$E(t) = \frac{C(t)}{\int_0^\infty C(t)\mathrm{d}t} \tag{3}$$

$$\tau = \int_0^\infty tE(t)\mathrm{d}t \tag{4}$$

To evaluate deviation from ideal plug flow, the elution curves were treated with dimensionless numbers. Dimensionless time (θ) and dimensionless RTD function ($E(\theta)$) were calculated as follows:

$$\theta = \frac{t}{\tau} \tag{5}$$

$$E(\theta) = \tau E(t) \tag{6}$$

For parametric RTD analysis, the dimensionless variance (σ^2) was further introduced, as follows:

$$\sigma^2 = \int_0^\infty (1-\theta)^2 E(\theta)\mathrm{d}\theta \tag{7}$$

Typical procedures for continuous-flow Michael addition

Michael addition of propionaldehyde to *trans*-β-nitrostyrene was performed under continuous-flow conditions using the **MPG** reactor (Scheme 1c). *trans*-β-Nitrostyrene (0.2 mol L^{-1}, 1.0 eq.), propionaldehyde (0.3 mol L^{-1}, 1.5 eq.), *p*-nitrophenol (0.02 mol L^{-1}, 10 mol%), and nitrobenzene (0.024 mol L^{-1}, 12 mol%, internal standard) were dissolved in toluene. The substrate solution was loaded in a glass syringe, and the syringe was attached to a syringe pump. The reactor was provided with fittings and attached to the syringe pump. At the control u, the substrate solution was continuously permeated through the **MPG** at 50 °C in a thermo-controlled incubator. The total elution volume of the substrate solution was normalized to be column volume (CV) as follows:

$$CV = \frac{Q}{V_M}t \tag{8}$$

The elution from the reactor was continuously collected and analyzed using HPLC (Fig. S3 and S4†) to determine the yield of product, turnover number (TON), turnover frequency (TOF), space–time yield (STY), enantiomeric excess (ee), and diastereomeric ratio (d.r.), as follows:

$$TON = \frac{\text{total amount of product}}{\text{loading of HJ-cat monomer}} \tag{9}$$

$$TOF = \frac{\Delta(\text{amount product at steady state})}{\text{loading of HJ-cat} \times t_{peak}} \tag{10}$$

$$STY = \frac{\text{production rate}}{V_M} \tag{11}$$

$$ee = \frac{\text{amount of major syn product} - \text{amount of minor syn product}}{\text{amount of major syn product} + \text{amount of minor syn product}} \times 100 \tag{12}$$

$$d.r. = \frac{\text{amount of syn product}}{\text{total amount of product}} \times 100 \tag{13}$$

where t_{peak} corresponds to the elution time at a peak top in the RTD curves. The reaction mixture was purified by normal-phase silica gel column chromatography (ethyl acetate/hexane), and the chemical structure of the product was identified using ^{1}H NMR (Fig. S2†).

Results and discussion

Characterization of MPG

The **MPG**s supporting HJ-cat were prepared through polymerization-induced phase separation in the presence of porogenic solvent (toluene/1-decanol).[31] To clarify the effect of swelling ability of the **MPG**s on the molecular diffusivity within the gel network, the different cross-linked structures in the **MPG**s were fabricated by varying the degree of cross-linking. The feed ratio of the DVB (X = 20, 40, or 60 wt%) was tuned to prepare a series of **MPG**s with different degrees of
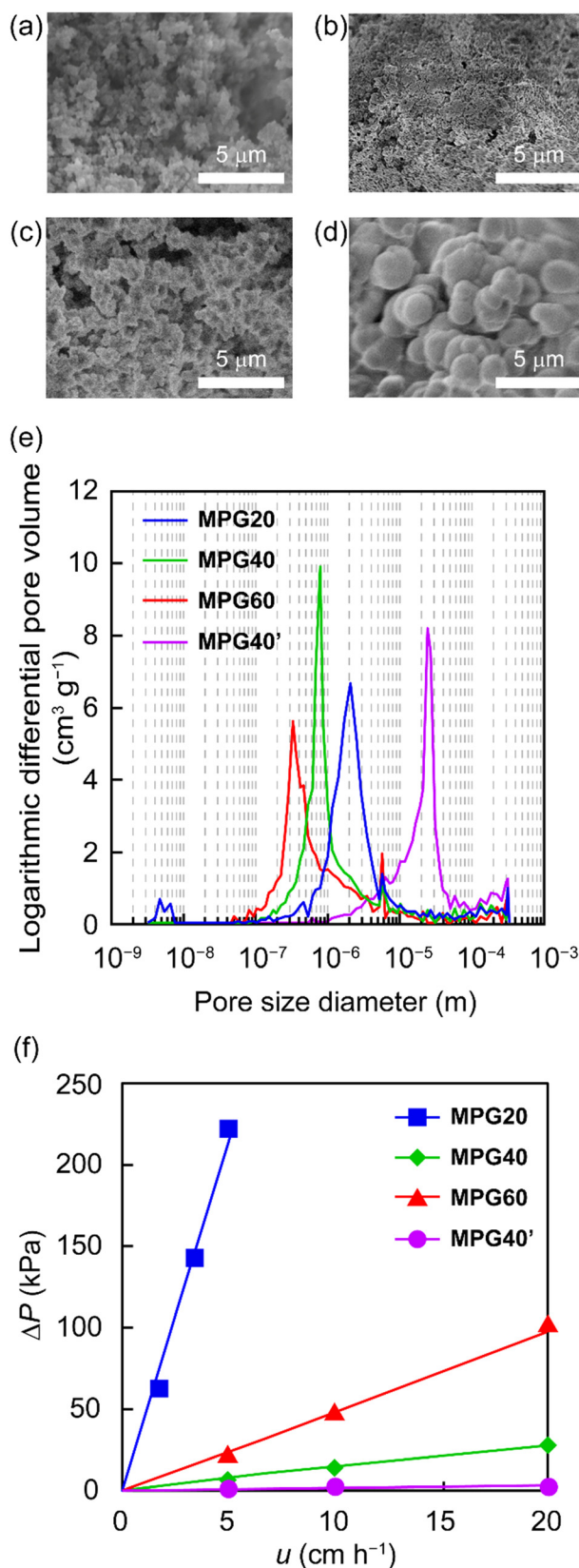
This journal is © The Royal Society of Chemistry 2025

React. Chem. Eng., 2025, **10**, 1038–1047 | **1041**

Fig. 2 FE-SEM images of (a) **MPG20**, (b) **MPG40**, (c) **MPG60**, and (d) **MPG40′**. (e) Pore-size distribution determined by MIP. (f) Continuous-flow permeability of the **MPG** reactors. Conditions: mobile phase = toluene, room temperature.

cross-linking (**MPG20**, **MPG40**, and **MPG60**). Further decreasing the degree of cross-linking of the monolith would not be suitable due to significant swelling and low permeability (described in a later section). All the **MPG**s were obtained as white solids with high yields (90–93% yield, Table S1, see ESI†). From EA for nitrogen, loading of HJ-cat in the **MPG**s was estimated to be 0.23–0.28 mmol g^{-1} (Table S1†). FE-SEM confirmed that the dried **MPG** consisted of aggregates of primary particles with diameters of 0.5–2.0 μm and interconnected pores between the particles (Fig. 2a–c). MIP revealed that all the **MPG**s had narrow and monomodal pore size (Fig. 2e). The median pore diameters (D_{med}) of the **MPG20**, **MPG40**, and **MPG60** were 2190, 800, and 340 nm, respectively (Table S2†). The porosity of the dried **MPG**s (ε_{dry}) was high enough to be 81–82%. Higher cross-linking degree caused decreasing sizes of the primary particles and pores, suggesting phase separation at an early stage due to suppressed swelling by cross-linking. Since all the **MPG**s possessed large through pores and high porosity, high permeability and excellent mass transfer could be obtained in continuous-flow systems.

Permeability of the MPG column

To evaluate the permeability of the **MPG**s in the continuous-flow system, toluene was fed through the column, and the ΔP at steady state was measured. Within the measured range, ΔP was proportional to u (Fig. 2f). Using Darcy's law, the values of k_D for **MPG20**, **MPG40**, and **MPG60** were calculated to be 1.8×10^{-15}, 5.6×10^{-14}, and 1.8×10^{-14} m^2, respectively. It has been reported that the k_D value of packed-bed silica particles ranges from 10^{-15} to 10^{-16} m^2.[32] The **MPG40** and **MPG60** exhibit excellent permeability, although the k_D value for **MPG20** was one order of magnitude lower. This might be due to significant swelling of **MPG20** in toluene due to less cross-linking, resulting in a reduced pore size in the swollen state. On the other hand, ΔP was proportional to u within the measured range, suggesting the absence of deformation of the **MPG** by hydrodynamic pressure. Using the **MPG** reactors, catalytic reactions in the continuous-flow systems could be successfully realized.

RTD and molecular diffusivity of pulse tracer through the MPG column

Mass transfer phenomena in the **MPG** reactors were evaluated using pulse tracer experiments with an in-line UV-vis spectrometer. Toluene was continuously fed to the **MPG** column (Q = 0.743 mL h^{-1}) and a pulse tracer (methyl red) was injected at the inlet of the **MPG** column. The absorbance of the tracer was continuously monitored with the in-line UV-vis spectrometer at a wavelength of 427 nm. In the elution curve of the tracer, a single peak was obtained for all the **MPG**s (Fig. 3a). The σ^2 values of the RTDs for the **MPG**s were calculated for deviation from an ideal plug flow (Fig. 3b). For **MPG20**, **MPG40**, and **MPG60**, the σ^2 values were 0.015, 0.018, and 0.124, respectively (Table 1). **MPG20** and **MPG40**
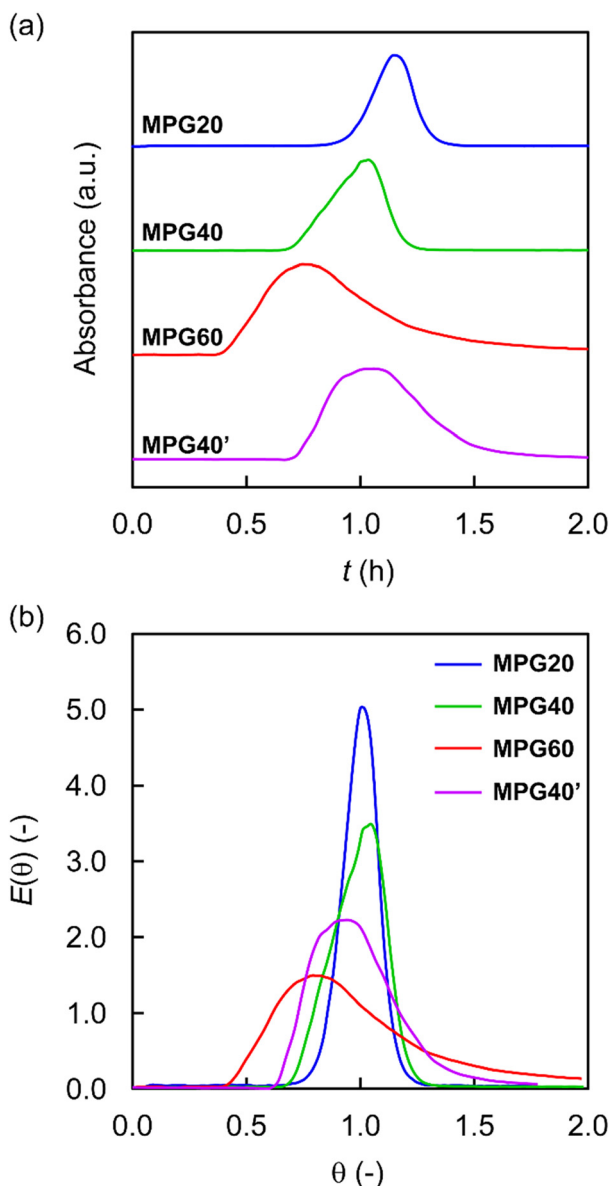
1042 | *React. Chem. Eng.*, 2025, **10**, 1038–1047

This journal is © The Royal Society of Chemistry 2025

Fig. 3 (a) Elution curves and (b) dimensionless RTD curves in pulse tracer experiments for the **MPG** columns. Conditions: tracer = methyl red (in EtOH, 1 g L^{-1}, 10 μL), mobile phase = toluene.

exhibited narrow RTDs, which were close to that of ideal plug flow.[33] On the other hand, **MPG60** showed a relatively broad RTD (Fig. 3b).

The molecular diffusion through the gel network of the **MPG**s was further evaluated from the RTD curves. It has been reported that the molecular diffusion of small molecules through the swollen gel is as fast as that in bulk liquid.[18] Hence, under continuous-flow conditions, tracer molecules could flow through the volume fraction of the swollen gel network in the **MPG** column. Using the elution time of the tracer, the porosity of the swollen **MPG** ($\varepsilon_{\text{swollen}}$) was calculated as follows:[34]

$$\varepsilon_{\text{swollen}} = \frac{Q t_{\text{peak}} - V_{\text{d}}}{V_{\text{M}}} \times 100 \qquad (14)$$

where V_{M} and V_{d} are the swollen **MPG** volume in the column and the dead volume from the injection valve to the UV-vis detector (0.113 mL), respectively. The $\varepsilon_{\text{swollen}}$ values for **MPG20**, **MPG40**, and **MPG60** were calculated as 100, 89, and 60%, respectively (Table 1). Notably, the **MPG** with a lower cross-linking degree exhibited a higher $\varepsilon_{\text{swollen}}$.

The amazingly high porosity in the swollen **MPG**s (up to 100% $\varepsilon_{\text{swollen}}$) indicated that the large volume fraction of the **MPG** column was accessible under continuous-flow conditions. The polystyrene-based **MPG**s functioned as organogels, which swelled in toluene. The swelling behavior of the **MPG** column allowed the small molecules to be transported to the interior of the gel network by diffusion under continuous-flow conditions. Furthermore, decreasing the cross-linking degree of the **MPG**s increased the $\varepsilon_{\text{swollen}}$ owing to low cross-linking of the gel network and good swelling in toluene. The swollen nature of the low-cross-linked **MPG**s accelerated the molecular diffusion of solutes through the gel network.[23–25] Additionally, the low-cross-linked gel might contribute to the small σ^2, which is close to ideal plug flow, owing to faster molecular diffusion. The narrow RTDs and fast molecular diffusion in the **MPG** columns could dramatically reduce the mass transfer resistance to catalytic sites, and hence lead to excellent catalytic efficiency in continuous-flow reactions.

Catalytic performance of MPG reactors in Michael addition

The catalytic performance of the **MPG** columns was evaluated in the asymmetric Michael addition of propionaldehyde (0.2 mol L^{-1}, 1.0 eq.) to *trans*-β-nitrostyrene (0.3 mol L^{-1}, 1.5 eq.) in toluene under continuous-flow conditions (Scheme 1c). Since the elution curves of the tracer showed different t_{peak}

Table 1 RTD variance (σ^2), porosity in swollen state ($\varepsilon_{\text{swollen}}$), diastereomeric ratio (d.r.), turnover frequency (TOF), and space–time yield (STY) for the **MPG**s

Catalyst	DVB [wt%]	σ^{2a} [–]	$\varepsilon_{\text{swollen}}{}^{a}$ [%]	d.r.^{b} [%]	TOF^{b} [h^{-1}]
MPG20	20	0.015	100	82	2.7
MPG40	40	0.018	89	81	2.3
MPG60	60	0.124	60	84	1.9
MPG40′	40	0.036	89	81	2.3

^{a} Determined from the pulse tracer experiments. ^{b} Determined at 6 CV during the continuous-flow Michael additions.
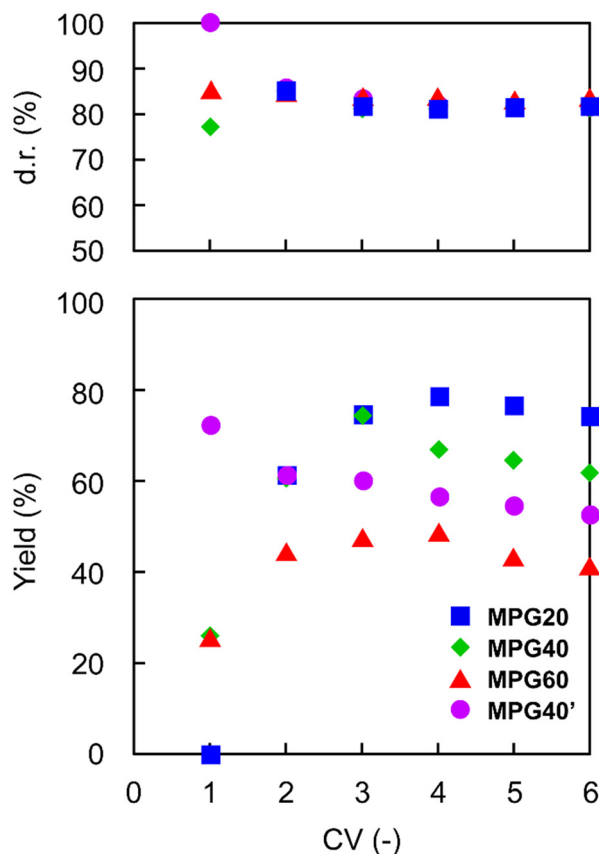
This journal is © The Royal Society of Chemistry 2025

React. Chem. Eng., 2025, **10**, 1038–1047 | **1043**

Fig. 4 Yield and d.r. in the continuous-flow Michael addition with the **MPG** reactors.

Fig. 5 (a) STY *vs.* $\varepsilon_{swollen}$ diagram. (b) Schematic of the **MPG**s with different cross-linking degree for high TOF and STY in continuous-flow reactions.

through each **MPG** column, the flow rate was adjusted to set the t_{peak} to 1.0 h, in order to fix a mean residence time. Along with permeation of the substrate solution, the yield of γ-nitroaldehyde gradually increased and reached an almost constant value within 6 CV (Fig. 4). The yields at steady state were 74–79%, 62–67%, and 41–49% for **MPG20**, **MPG40**, and **MPG60**, respectively. In addition, all the **MPG**s processed asymmetric Michael additions with high selectivity, to give a d.r. of 81–84% (Fig. 4 and Table 1). The ee was 91% for **MPG20** in 1–6 CV. At 6 CV, the TOFs for **MPG20**, **MPG40**, and **MPG60** were estimated to be 2.7, 2.3, and 1.9 h^{-1}, respectively (Table 1). To evaluate the productivity of the **MPG** reactors, STYs were calculated. At 6 CV, the STYs for **MPG20**, **MPG40**, and **MPG60** were 167, 123, and 55 mmol h^{-1} L^{-1}, respectively (Table 1). Interestingly, decreasing the DVB content resulted in dramatic improvements, with 1.4- and 3.0-fold increases in the TOF and STY, respectively. Clearly, the higher STYs of the **MPG**s strongly relate to the higher $\varepsilon_{swollen}$ of the gel.

In the continuous-flow Michael addition, a decreased degree of cross-linking of the **MPG** significantly increased the catalytic activity (Fig. 4). From the RTD tests, a lower degree of cross-linking of the **MPG** exhibited a higher $\varepsilon_{swollen}$, meaning that a larger volume fraction of the gel network was available for molecular diffusion of the reactants. As a result, efficient contact between catalysts and reactants was realized
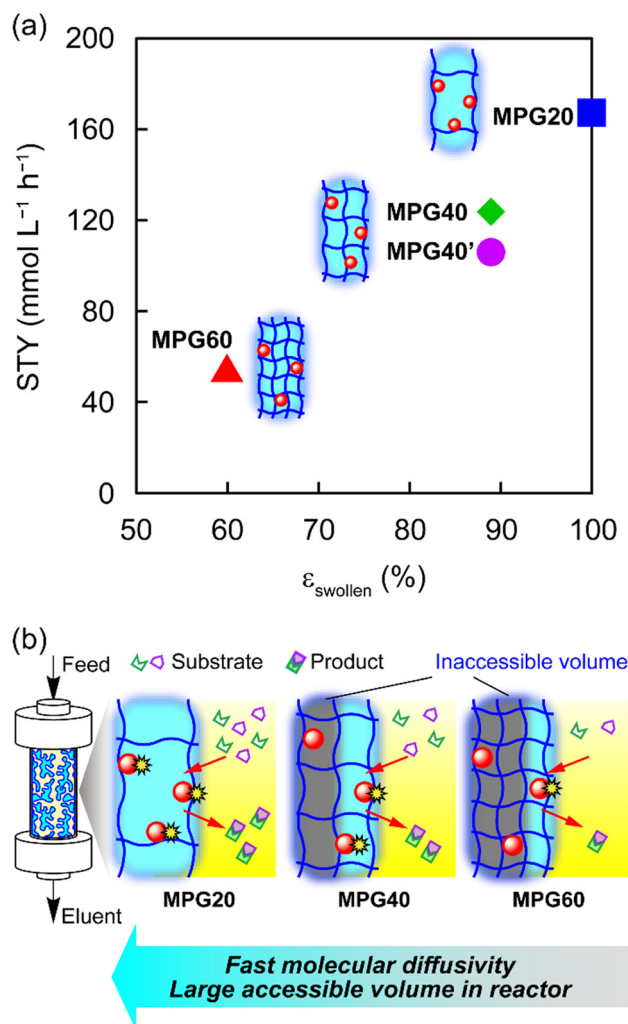
within the gel network of the **MPG**, leading to an excellent TOF. Furthermore, a higher $\varepsilon_{swollen}$ of the **MPG** corresponded to larger accessibility in the reactor volume available for catalytic reactions. This feature of the **MPG**s minimized the inaccessible volume of the reactor, which significantly improved the STY with increase in the $\varepsilon_{swollen}$ (Fig. 5a and b). Design of immobilized catalysts based on a swollen support with higher $\varepsilon_{swollen}$ is a powerful method for enhancing the catalytic efficiency and productivity of the continuous-flow reactors.

Effect of porous structure of the MPG on catalytic performance

The effects of the surface morphologies of the **MPG**s on the catalytic performance were confirmed. Compared with the original **MPG**, a reference **MPG** with different macroporous structures but the same degree of cross-linking in the gel was prepared. For preparation of the reference **MPG**, the

composition of the porogenic solvent was varied (toluene/1-decanol = 20:80 w/w), while the feed ratio of the DVB was fixed at 40 wt%. Compared with **MPG40**, the resulting **MPG40′** was expected to have a different macroporous structure but the same degree of cross-linking (X = 40 wt%). The **MPG40′** showed a smaller specific surface area than **MPG40** (1 vs. 17 m^2 g^{-1}, Table S2†). The pulse experiment was performed, giving an $\varepsilon_{swollen}$ of 89% for **MPG40′** (Fig. 3 and Table 1), which was the same as for the original **MPG40** (89%). The σ^2 of **MPG40′** (0.036, Table 1) was slightly larger than that of the **MPG40** (0.018). In the continuous-flow Michael addition, **MPG40′** exhibited comparable TOF, STY, and d.r. (2.3 h^{-1}, 106 mmol h^{-1} L^{-1}, and 81%, Fig. 4 and Table 1) values to those of **MPG40** (2.3 h^{-1}, 123 mmol h^{-1} L^{-1}, and 81%). These results suggested little effect of surface morphology on the molecular diffusivity through the **MPG** and on catalytic performance in continuous-flow reactions.

Since the surface area of the **MPG** had little influence on its catalytic performance, it could be anticipated that most of the catalytic sites were preferentially located in the interior rather than on the exterior of the gel phase in the **MPG**s.[35,36] In this case, efficient access of reactants toward the interior of the gel network in the **MPG**s improved the catalytic activity due to the increased number of the catalysts. Thus, the degree of cross-linking of the **MPG**s had a critical effect on their catalytic efficiency and reactor performance in the continuous-flow asymmetric reaction.

Comparison of MPG reactors with GP reactors

Finally, to emphasize the importance of the porous nature and monolithic structure of the **MPG**, a reference catalyst was prepared from gel particles (**GP**s). The polystyrene-based **GP** supporting HJ-cat was synthesized through a suspension copolymerization process (DVB 40 wt%, Fig. S5, see ESI†). The resulting **GP** was sieved into particles ranging in size from 420 to 640 μm in diameter, and packed into a stainless steel column. In the RTD curve for the **GP** column, a broader peak was obtained than for the **MPG40** column (Fig. 6a). The

σ^2 value for the **GP** column was calculated as 0.086, which was larger than that for the **MPG40** column (0.018, Fig. 6b). Additionally, the $\varepsilon_{swollen}$ for the **GP** column was estimated to be 65%, which is fairly low compared to that of **MPG40** (89%). In the continuous-flow Michael addition, the d.r. and TOF for the **GP** column were 77–81% and 1.9 h^{-1}, respectively. The higher TOF of the **MPG40** (2.3 h^{-1}, Table 1) than for **GP** (1.9 h^{-1}) was noted. Moreover, the STY for the **GP** column (99 mmol h^{-1} L^{-1}, Fig. 6c) was lower than that for **MPG40** (123 mmol h^{-1} L^{-1}). The narrow pore-size distribution (Fig. 2e) and the small primary particles (0.5–2.0 μm diameters, Fig. 2a–d) of the **MPG** were beneficial for a narrow RTD and fast diffusivity through the gel network. These characteristic of the **MPG** contribute to its amazingly high $\varepsilon_{swollen}$, resulting in the high catalytic efficiency and productivity of the reactor.

Conclusions

In conclusion, monolithic porous gels, **MPG**s, were developed as support materials for immobilization of HJ-cat in continuous-flow asymmetric catalysis. Pulse tracer experiments were performed to determine RTD and molecular diffusivity of the reactants through the **MPG** reactor. The variance, σ^2, and porosity in swollen state, $\varepsilon_{swollen}$, were calculated, and greatly influenced the catalytic performance in the continuous-flow Michael addition. The **MPG** with the lowest degree of cross-linking achieved both a small σ^2 and large $\varepsilon_{swollen}$, demonstrating ideal plug flow and remarkably high molecular diffusivity. This led to dramatic improvement in the catalytic performance of the **MPG** column, where the TOF and STY were up to 1.4 and 3.0 times higher, respectively. This was attributed to the increased number of effective catalytic sites owing to enhanced molecular diffusivity through the gel network in the **MPG** catalysts. These findings provide a design criterion relating to swelling of immobilized catalysts for improving the catalytic performance of continuous-flow reactors.
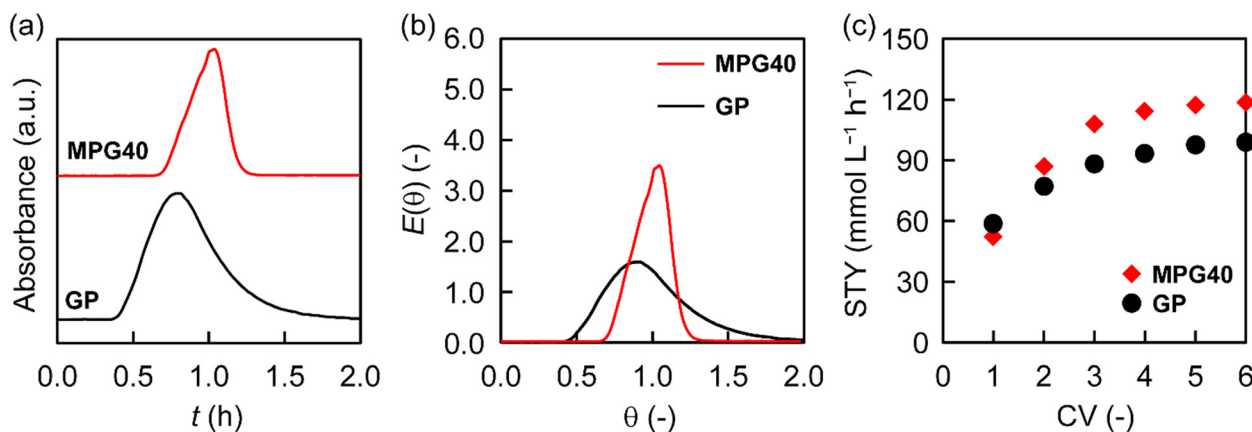

Fig. 6 (a) Elution curves and (b) dimensionless RTD curves of pulse tracers. (c) STY of **MPG40** and the **GP** in the continuous-flow Michael addition. The **MPG40** and **GP** were prepared with the same feed ratio of DVB content (40 wt%) as that for **MPG40**.

Data availability

The authors confirm that the data supporting the findings of this study are available within the article and its ESI† materials.

Author contributions

H. Shigeeda, H. Matsumoto, and Y. Miura designed the experiments. H. Shigeeda performed the experiments. H. Shigeeda, H. Matsumoto, and Y. Miura wrote the manuscript. M. Nagao made contributions to the discussions during this work. All authors have given approval to the final version of the manuscript.

Conflicts of interest

There are no conflicts to declare.

Acknowledgements

References

1 S. V. Ley, Y. Chen, A. Robinson, B. Otter, E. Godineau and C. Battilocchio, A comment on continuous flow technologies within the agrochemical industry, *Org. Process Res. Dev.*, 2021, **25**, 713–720.

2 A. Gioiello, A. Piccinno, A. M. Lozza and B. Cerra, The medicinal chemistry in the era of machines and automation: recent advances in continuous flow technology, *J. Med. Chem.*, 2020, **63**, 6624–6647.

3 G. Gambacorta, J. S. Sharley and I. R. Baxendale, A comprehensive review of flow chemistry techniques tailored to the flavours and fragrances industries, *Beilstein J. Org. Chem.*, 2021, **17**, 1181–1312.

4 J. Britton and C. L. Raston, Multi-step continuous-flow synthesis, *Chem. Soc. Rev.*, 2017, **46**, 1250–1271.

5 R. L. Hartman, J. P. McMullen and K. F. Jensen, Deciding Whether To Go with the Flow: Evaluating the Merits of Flow Reactors for Synthesis, *Angew. Chem., Int. Ed.*, 2011, **50**, 7502–7519.

6 C. Wiles and P. Watts, Continuous flow reactors: a perspective, *Green Chem.*, 2012, **14**, 38–54.

7 R. Porta, M. Benaglia and A. Puglisi, Flow chemistry: recent develop- ments in the synthesis of pharmaceutical products, *Org. Process Res. Dev.*, 2016, **20**, 2–25.

8 P. Kumar, A. Das and B. Maji, Phosphorus containing porous organic polymers: synthetic techniques and applications in organic synthesis and catalysis, *Org. Biomol. Chem.*, 2021, **19**, 4174–4192.

9 T. Drake, P. Ji and W. Lin, Site Isolation in Metal–Organic Frameworks Enables Novel Transition Metal Catalysis, *Acc. Chem. Res.*, 2018, **51**, 2129–2138.

10 F. Svec and J. M. J. Frechet, New Designs of Macroporous Polymers and Supports: From Separation to Biocatalysis, *Science*, 1996, **273**, 205–211.

11 F. Svec, Porous polymer monoliths: amazingly wide variety of techniques enabling their preparation, *J. Chromatogr. A*, 2010, **1217**, 902–924.

12 V. Chiroli, M. Benaglia, A. Puglisi, R. Porta, R. P. Jumde and A. Mandoli, A chiral organocatalytic polymer-based monolithic reactor, *Green Chem.*, 2014, **16**, 2798–2806.

13 A. Sachse, A. Galarneau, F. Fajula, F. Di Renzo, P. Creux and B. Coq, Functional silica monoliths with hierarchical uniform porosity as continuous flow catalytic reactors, *Microporous Mesoporous Mater.*, 2011, **140**(1–3), 58–68.

14 J. Lee and J. Y. Chang, A hierarchically porous catalytic monolith prepared from a Pickering high internal phase emulsion stabilized by microporous organic polymer particles, *Chem. Eng. J.*, 2020, **381**, 122767.

15 L. Tan and B. Tan, Functionalized hierarchical porous polymeric monoliths as versatile platforms to support uniform and ultrafine metal nanoparticles for heterogeneous catalysis, *Chem. Eng. J.*, 2020, **390**, 124485.

16 Y. Osada and J. P. Gong, Soft and Wet Materials: Polymer Gels, *Adv. Mater.*, 1998, **10**, 827–837.

17 M. A. Kuzina, D. D. Kartsev, A. V. Stratonovich and P. A. Levkin, Organogels versus Hydrogels: Advantages, Challenges, and Applications, *Adv. Funct. Mater.*, 2023, **33**, 2301421.

18 P. C. Carman and R. A. W. Haul, Measurement of diffusion coefficients, *Proc. R. Soc. A.*, 1954, **222**, 109–118.

19 K. Hawkins, A. K. Patterson, P. A. Clarke and D. K. Smith, Catalytic Gels for a Prebiotically Relevant Asymmetric Aldol Reaction in Water: From Organocatalyst Design to Hydrogel Discovery and Back Again, *J. Am. Chem. Soc.*, 2020, **142**, 4379–4389.

20 R. Porcar, M. I. Burguete, P. Lozano, E. Garcia-Verdugo and S. V. Luis, Supramolecular Interactions Based on Ionic Liquids for Tuning of the Catalytic Efficiency of (L)-Proline, *ACS Sustainable Chem. Eng.*, 2016, **4**, 6062–6071.

21 A. Lu, D. Moatsou, D. A. Longbottom and R. K. O'Reilly, Tuning the catalytic activity of L-proline functionalized hydrophobic nanogel particles in water, *Chem. Sci.*, 2013, **4**, 965–969.

22 C. J. Schmiegel, R. Baier and D. Kuckling, Direct Asymmetric Aldol Reaction in Continuous Flow Using Gel-Bound Organocatalysts, *Eur. J. Org. Chem.*, 2021, **17**, 2578–2586.

23 H. Matsumoto, H. Seto, T. Akiyoshi, M. Shibuya, Y. Hoshino and Y. Miura, Macroporous gel with a permeable reaction platform for catalytic flow synthesis, *ACS Omega*, 2017, **2**, 8796–8802.

24 H. Matsumoto, H. Seto, T. Akiyoshi, M. Shibuya, Y. Hoshino and Y. Miura, Macroporous monolith with polymer gel

1046 | *React. Chem. Eng.*, 2025, **10**, 1038–1047

This journal is © The Royal Society of Chemistry 2025

matrix as continuous-flow catalytic reactor, *Chem. Lett.*, 2017, **46**, 1065–1067.

25 H. Matsumoto, H. Hattori, M. Nagao, Y. Hoshino and Y. Miura, Continuous-Flow Asymmetric Aldol Addition Using Immobilized Chiral Catalyst on Organogel-Based Porous Monolith, *J. Chem. Eng. Jpn.*, 2024, **57**, 2384402.

26 Y. Hayashi, H. Gotoh, T. Hayashi and M. Shoji, Diphenylprolinol silyl ethers as efficient organocatalysts for the asymmetric Michael reaction of aldehydes and nitroalkenes, *Angew. Chem., Int. Ed.*, 2005, **44**, 4212–4215.

27 K. A. Jørgensen, M. Johannsen, S. Yao, H. Audrain and J. Thorhauge, Catalytic asymmetric addition reactions of carbonyls. A common catalytic approach, *Acc. Chem. Res.*, 1999, **32**, 605–613.

28 Y. Hayashi, S. Hattori and S. Koshino, Asymmetric Flow Reactions Catalyzed by Immobilized Diphenylprolinol Alkyl Ether: Michael Reaction and Domino Reactions, *Chem. – Asian J.*, 2022, **17**, e202200314.

29 H. Ochiai, A. Nishiyama, N. Haraguchi and S. Itsuno, Polymer-Supported Chiral Cis-Disubstituted Pyrrolidine Catalysts and Their Application to Batch and Continuous-Flow Systems, *Org. Process Res. Dev.*, 2020, **24**, 2228–2233.

30 V. Sans, N. Karbass, M. I. Burguete, E. García-Verdugo and S. V. Luis, Residence time distribution, a simple tool to understand the behaviour of polymeric mini-flow reactors, *RSC Adv.*, 2012, **2**, 8721–8728.

31 C. Viklund, F. Svec, J. M. J. Fréchet and K. Irgum, Preparation of porous poly(styrene-co-divinylbenzene) monoliths with controlled pore size distributions initiated by stable free radicals and their pore surface functionalization by grafting, *Chem. Mater.*, 1996, **8**, 744–750.

32 S. Jung, S. Ehlert, J. A. Mora, K. Kraiczek, M. Dittmann, G. P. Rozing and U. Tallarek, Packing density, permeability, and separation efficiency of packed microchips at different particle-aspect ratios, *J. Chromatogr. A*, 2009, **1216**, 264–273.

33 S. R. L. Gobert, S. Kuhn, L. Braeken and L. C. J. Thomassen, Characterization of milli-and microflow reactors: mixing efficiency and residence time distribution, *Org. Process Res. Dev.*, 2017, **21**, 531–542.

34 J. Urban, S. Eeltink, P. Jandera and P. J. Schoenmakers, Characterization of polymer-based monolithic capillary columns by inverse size-exclusion chromatography and mercury-intrusion porosimetry, *J. Chromatogr. A*, 2008, **1182**, 161–168.

35 B. Altava, M. I. Burguete, E. García-Verdugo and S. V. Luis, Chiral catalysts immobilized on achiral polymers: effect of the polymer support on the performance of the catalyst, *Chem. Soc. Rev.*, 2018, **47**, 2722–2771.

36 S. Itsuno and M. M. Hassan, Polymer-immobilized chiral catalysts, *RSC Adv.*, 2014, **4**, 52023–52043.

This journal is © The Royal Society of Chemistry 2025

React. Chem. Eng., 2025, **10**, 1038–1047 | **1047**